Computational Investigation of Effects of Ligand Architecture on Homolytic Bond Cleavage and Electronic Structure of Molecular Bismuth Compounds

Introduction

Transition metals have inevitable downsides due to their affordability and toxicity

Transition metals are widely used in a variety of catalytic reactions due to their excellent ability to undergo redox cycles and facilitate complex bond transformations. Also, the exceptional ability of transition metal catalysts originates from single-electron transfer reactions, triggering radical reactions (Demarteau et al., 2016). Such catalysts are essential in both industrial and academic synthetic chemistry because of high efficiency and broad substrate scope.

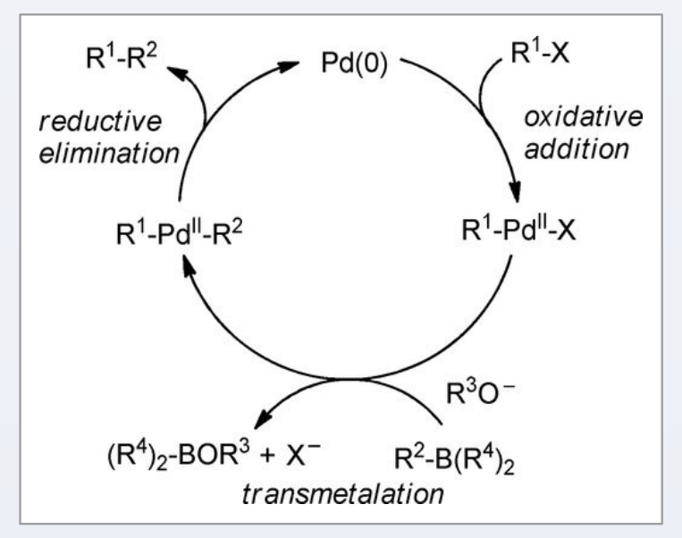

Figure 1: General Scheme of Suzuki-Miyaura Cross-Coupling Catalyzed by Palladium Catalysts (Jana et. al., 2011)

However, many transition-metal catalysts are expensive, toxic, and not environmentally-friendly; for example, many transition metals such as palladium have shown to have detrimental effects on overall human health such as hepatitis, myocarditis, and rheumatoid arthritis (Jomova et al., 2024). Such factors limit sustainable use and poses challenges for green chemistry applications

Main-Group metals provide alternative to transition metal catalysts

Thus, the recent efforts have focused on developing main-group metal complexes (e.g., aluminum, gallium, indium, tin, bismuth, etc.) as sustainable alternatives to transition-metal catalysts. Normally, such lighter elements are not the best at mediating electron-transfer reactions very well, which is why main-group elements haven't been used much in catalysis.

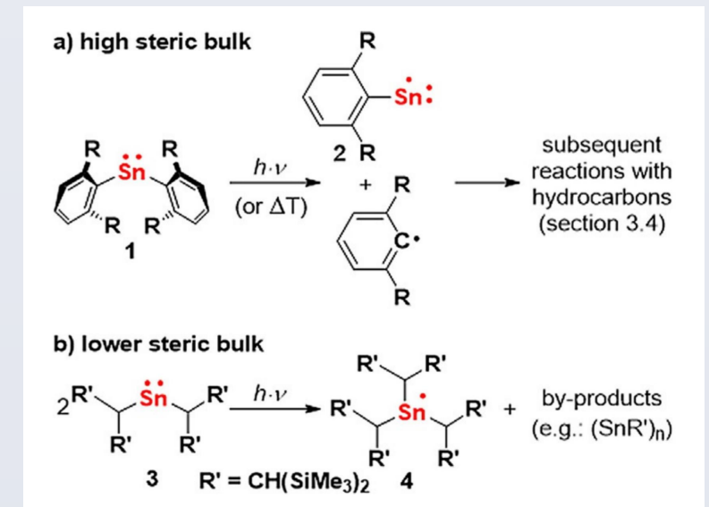

Figure 2: Sn Radical Species for Catalysis of Electron-Transfer Reactions (Lichtenberg, 2020)

However, carefully designed ligand frameworks, the molecules surrounding the metal, modify change how the metal behaves. By building ligands bulky enough to protect the metal, it is possible to control its electronic environment and reactivity. Specifically, redox-active ligands enable reversible electron transfer without the requirement for inherently redox-active metals. Furthermore, delocalization of spin density in π-conjugated electron systems enables selective bond formation and facilitates multi-electron transformations, historically reserved for transition metals (Lichtenberg, 2020). Recent advances in ligand design have enabled main-group elements such as aluminum, boron, and silicon to participate in oxidative addition and reductive elimination pathways, mimicking transition-metal-like reactivity as shown in the **Figure 1** (Crimmin et al., 2018). These developments highlight the growing potential of main-group metal catalysts as a sustainable and cost-effective alternative to traditional transition-metal systems.

Bismuth goes through different redox catalysis pathways

Many current studies have focused on mechanistic investigations of bismuth-mediated redox catalysis, examining how electronic structure and oxidation states influence reaction pathways. Unlike many common elements, bismuth is shown to be effective in mediating redox catalysis due to its access to multiple oxidation states—Bi(III)/Bi(I), Bi(III)/Bi(II), and even Bi(V)/BI(III)—enabling diverse radical and redox transformations (Cornella & Moon, 2022). According to mechanistic studies, such transformations often proceed via single-electron transfer processes, where radical intermediates with lone electron mediate bond formations and regenerate the catalytically active bismuth species (Yang et al., 2023). Despite such efforts, many molecular bismuth intermediates remains unstable especially at radical states due to dimerization of bismuth free radical species, highlighting importance of designing optimal ligand architectures to stabilize the molecular complex and suppress undesired side reactions. The general strategy is adding electron-donating substituents to enhance radical delocalization and π-conjugated frameworks to facilitate spin density distribution across the ligand, minimizing localized radical character at the bismuth center, thus, preventing undesirable side reactions. Additionally, the substituents added to phenyl rings of the ligand architecture affects the favorability of homolysis of molecular bismuth complexes, directly determining the likelihood of formation of free radicals intermediates.

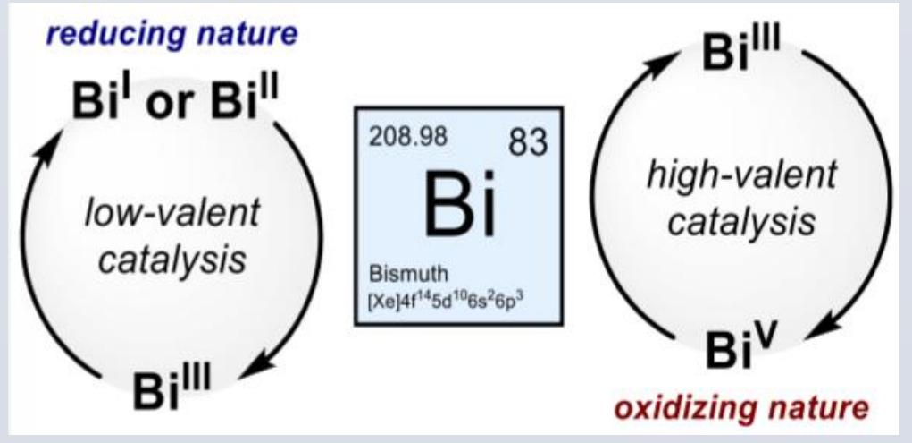

Figure 3: General Scheme of Bismuth Redox Catalysis (Cornella et al., 2022)

Research Question

Research Question: How do different substituents (–CF_3, –NH_2, –OCH_3, –CH_3, –NO_2, –isopropyl), their positions on the aryl rings (ortho, para, or meta depending on bridging), and the presence of bridging groups (–CH_2, –S, –SO_2) influence the electronic structure, quasi-atomic orbital (QUAO) profiles, and homolytic bond dissociation energies in organobismuth complexes?

Identifying High-Priority Computational Targets

Based on previous density functional theory (DFT) studies of organobismuth complexes with various ligands, the optimal molecular structures were identified by comparing the homolytic bond dissociation energies (BDE) of Mn-Bi bonds (Martinez, 2025). The BDE was calculated from single-point energies of optimized singlet and doublet states before and after the homolytic cleavage. The most favorable ligand candidates are shown in **Figure 4**. Among these, **Compound 3**, featuring methyl bridge between phenyl groups, exhibits the lowest BDE of 26.4 kcal mol^{-1} (Martinez, 2025). Other geometries such as **Compound 2** and **4** show slightly higher BDEs of 26.8 kcal mol^{-1} and 26.7 kcal mol^{-1}, respectively (Martinez, 2025). Although **Compound 1** displays significantly higher BDE of 29.7 kcal mol^{-1}, it remains under consideration for further DFT screening due to its structural simplicity and absence of bridging groups; substituents will be added to the aryl rings to observe electronic effects of substituents.

Previous mechanistic studies on the photochemically induced radical dehydrocoupling of diorgano(bismuth)chalcogenides, [Bi(di-aryl)EPh], with TEMPO have underscored the pivotal influence of the chalcogen substituent (E = S, Se, Te) on the reaction pathway and efficiency. The photosensitivity of such complexes increases with the atomic numbers of E, reflecting enhanced spin-orbit coupling in heavier chalcogens, whereas the selectivity improves with lighter analogues due to reduced nonradiative decay and tighter control over radical formation (Ramler, 2020). Consequently, SPh is identified as an optimal ligand, offering favorable balance between photoreactivity and selectivity for homolytic cleavage.

Figure 5 shows the fundamental computational candidates with functional groups (R_1) introduced on the aryl rings to probe electronic effects. Electron-donating groups (e.g., OCH_3) and electron-withdrawing groups (e.g., NO_2) are expected to influence the electronic properties of the molecules differently. The bridging groups enumerated in **Figure 4** will be systematically incorporated to examine the influence on the electronic distribution and steric environment of the complexes as shown in **Figure 6.**

Among these computational candidates, only the fundamental structures shown in **Figure 5** were fully analyzed, from density functional theory (DFT) calculations through quasi-atomic orbital (QUAO) analysis. The candidate containing a sulfur bridging group (R = S in **Figure 6**) was subjected only to DFT screening to evaluate homolytic bond dissociation energies (BDEs) for comparison with unbridged structures. Variations in substituents and bridging motifs were treated as independent variables, while a baseline model with X = H and no bridging group served as the control.

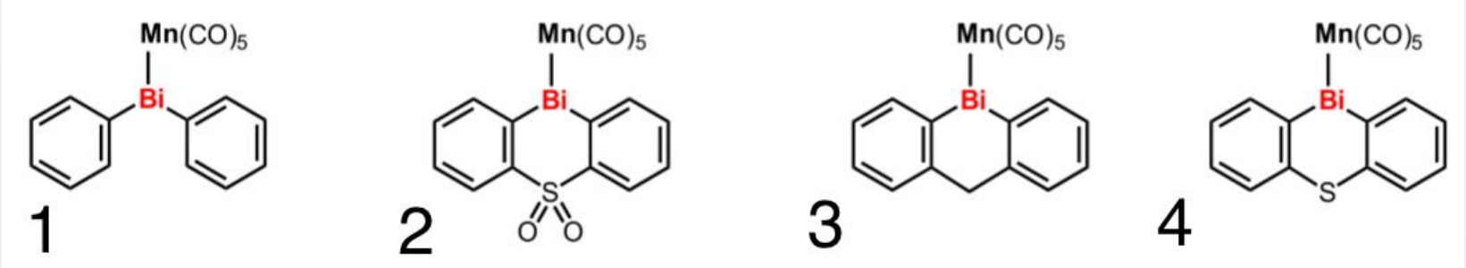

Figure 4: Molecular bismuth complexes with favorable homolytic bond dissociation energies obtained from DFT studies (Martinez et. al., 2025)

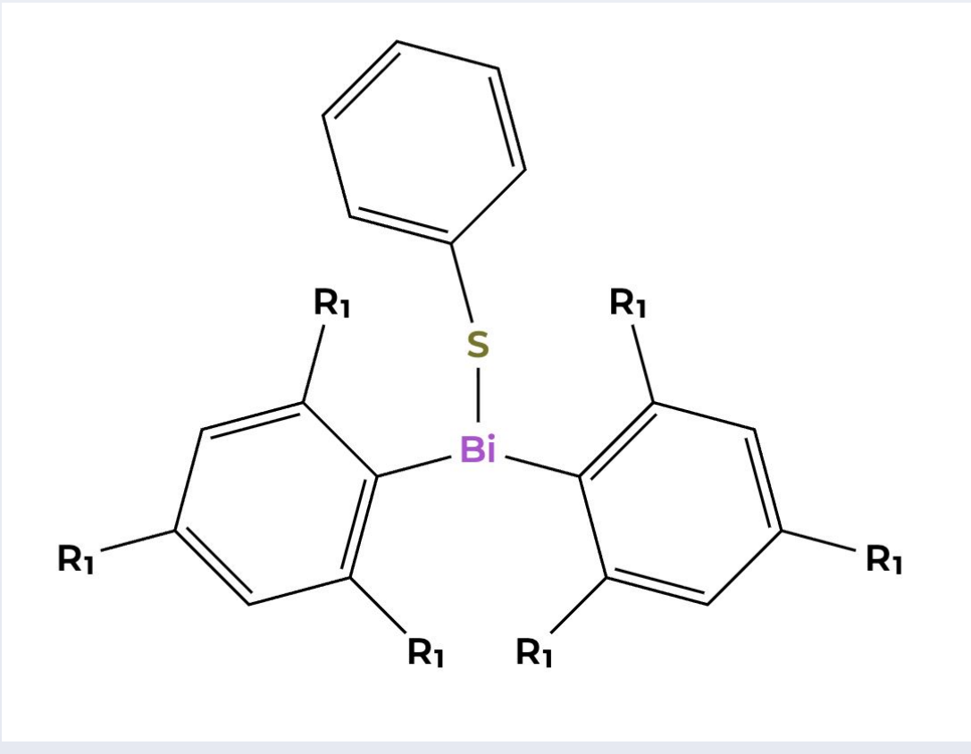

Figure 5: Bi(di-aryl)SPh with different functional groups attached to (e.g., R_1 = CF_3, –NH_2, –OCH_3, –CH_3, –NO_2, –H, –isopropyl)

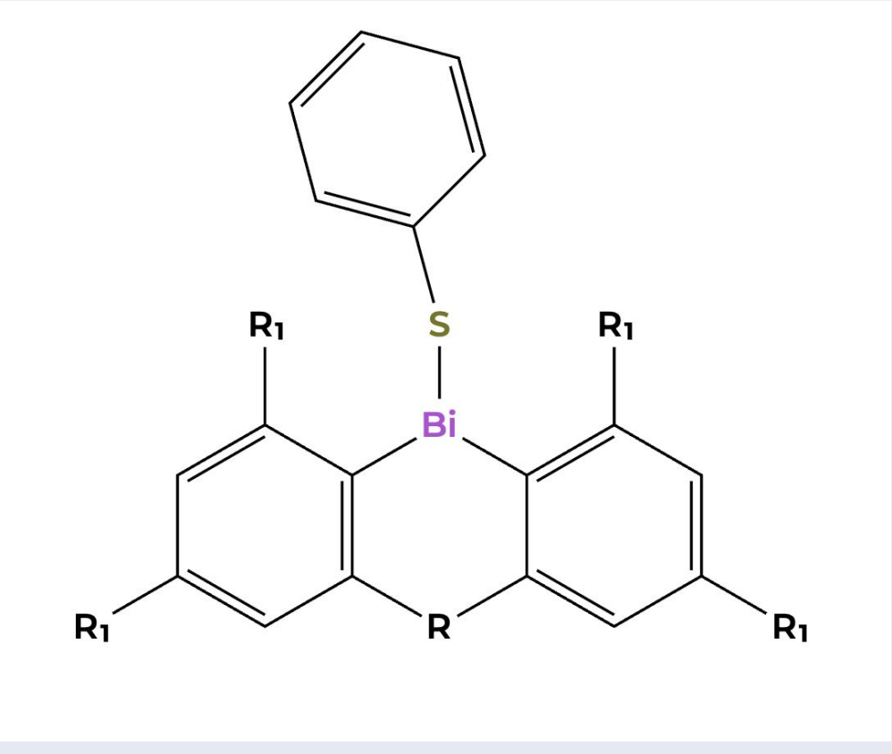

Figure 6: Bi(di-aryl)SPh with different bridging groups (e.g., R = –CH_2, –S, –SO_2) along with variable functional group R_1

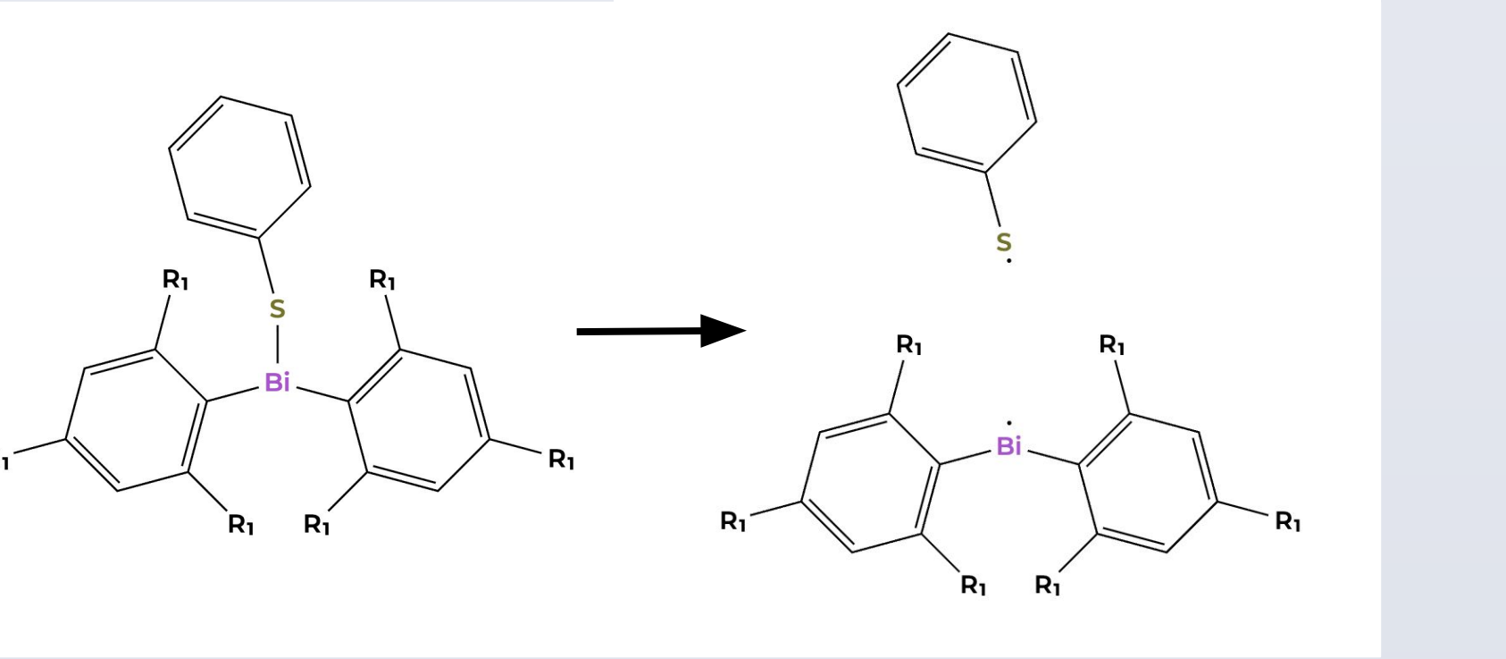

Figure 5: Homolytic cleavage of Bi(di-aryl)SPh with Bi(I) center into Bi(II) and phenylthiyl radicals

Experimental Design and Methodology: Computational Chemistry

All computations were performed with the ORCA 6.0 program package. To determine the ground-state geometries of the Bi(III) complexes and to closely approximate experimental conditions, geometry optimizations were performed in gas phase with def2-TZVP and def2-SVPD basis sets; def2-TZVP basis set will be primarily used due to its ability to yield the most accurate ground-state geometries, but other cheaper basis sets such as def2-SVPD and def2-SVP may be employed before performing final optimization with def2-TZVP to minimize the computational cost. Relativistic effects for bismuth will be treated with the corresponding effective core potential (ECP). The exchange–correlation functionals such as M06-L were employed with symmetry constraints utilizing tight self-consistent field (SCF) convergence criteria and tight numerical integration grid settings to ensure accurate evaluation. The M06-L functional, combined with the def2-TZVP basis set and solvent -models, has been reported to yield the most accurate ground-state geometries when compared to experimental X-ray crystallographic data (Martins, 2024). Therefore, the M06-L/def2-TZVP/ECP level of theory was primarily used for all geometry optimizations.

Upon convergence, analytic vibrational frequency analyses was performed to confirm that the optimized geometries correspond to true ground-state minima on the potential energy surface. Any stationary points are classified as true local minima only if all computed harmonic vibrational frequencies are real; the presence of one or more imaginary frequencies indicate the presence of at least one negative eigenvalue of the mass-weighted Hessian matrix, implying convergence to a first-order saddle point rather than a local minimum. The specific options for all of the calculations above are listed in **Figure 6**.

In cases where spurious imaginary modes are observed despite the use of tight integration grids, or when frequency calculations fail to converge, auxiliary basis set parameters will be adjusted to mitigate linear dependency and numerical instability. Notably, single-point energies exhibited non-negligible deviations (|ΔE| = 1.93 kJ/mol) depending on the auxiliary basis set employed as illustrated in **Figure 7**. To maintain consistency across all DFT calculations, the identical auxiliary basis set will be therefore applied for both geometry optimizations and subsequently frequency analyses. By default, AutoAux protocol of ORCA is primarily utilized to generate appropriate auxiliary basis sets; however, predefined basis sets such def2/j sets was employed instead where explicitly defined Coulomb fitting bases improve SCF stability and reduce residual integration errors.

Following confirmation of true local minima, the homolytic bond dissociation energies (BDEs) of the Bi-SPh bonds were determined from single-point energy evaluations on the optimized single doublet states. The mechanism of homolytic cleavage is shown in **Figure 5.** The BDE values will be obtained according to:

$$\mathrm{BDE} = \mathrm{E}_{\mathrm{Bi(di-aryl)\cdot}} + \mathrm{E}_{\mathrm{SPh\cdot}} - \mathrm{E}_{\mathrm{Bi(di-aryl)SPh}}$$

where BDE is determined by the total electronic energy of the optimized closed-shell singlet Bi(III) complex, and the total energies of the resulting Bi-centered and phenylthiyl radicals. **The homolytic BDE is one of the key dependent variables, alongside the QUAO data discussed below.**

Quasi-Atomic Bonding Orbitals (QUAO) are localized orbitals obtained by projecting delocalized molecular orbitals (MOs) onto sets of atomic-centered orbitals, providing a bridge between fully delocalized MOs and atomic orbital interpretations of bonding. QUAO provides insight into electron density distribution and bond character, bridging the gap between fully delocalized molecular orbitals and atomic-centered interpretations; specifically, it provides quantitative analysis of kinetic bond order, electron occupation numbers, and hybridization character, reflecting the contributions of individual atomic orbitals to bonding and antibonding interactions (Ruedenberg et al., 2020). QUAO analysis enables the assessment of bond strengths, radical character, and electronic delocalization in complex molecular systems, making it particularly useful for studying reactive Bi-centered radicals. **The resulting QUAO data provides quantitative insight into the distribution of electron density, hybridization character at metal center, and degree of orbital delocalization across the ligand framework, all of which are dependent variables to analyze as shown in FIgure 9.**

Ground-State Geometry Optimization	! m06l def2-tzvp def2/j printbasis TIGHTOPT DEFGRID3 verytightscf
Vibrational Frequency Analysis	! m06l def2-tzvp def2/j printbasis freq DEFGRID3 verytightscf

Figure 6: Computational parameters used for ground-state geometry optimization and vibrational frequency analysis in ORCA

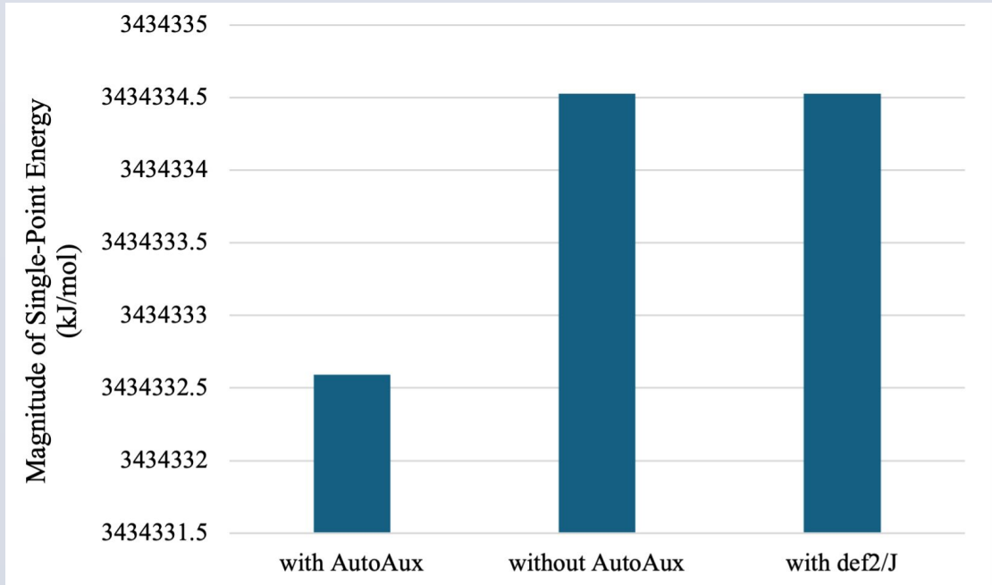

Figure 7: Difference in single point energies for different auxiliary basis sets (Shin, 2025)

Mathematical Background: Quasi-Atomic Orbital

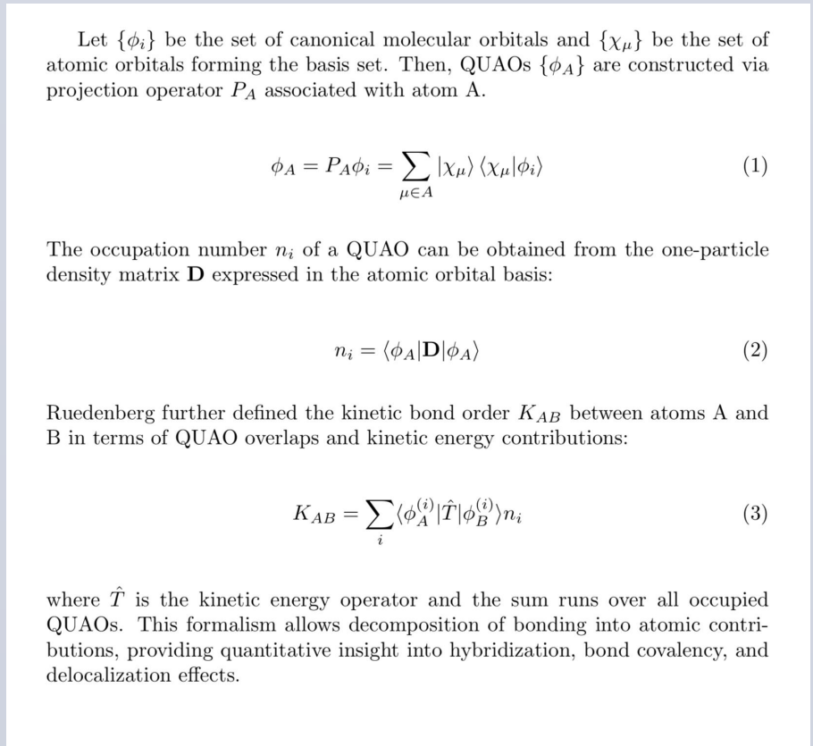

Let $\{\phi_i\}$ be the set of canonical molecular orbitals and $\{\chi_\mu\}$ be the set of atomic orbitals forming the basis set. Then, QUAOs $\{\phi_A\}$ are constructed via projection operator P_A associated with atom A.

$$\phi_A = P_A\phi_i = \sum_{\mu\in A} |\chi_\mu\rangle\langle\chi_\mu|\phi_i\rangle \qquad (1)$$

The occupation number n_i of a QUAO can be obtained from the one-particle density matrix $\mathbf{D}$ expressed in the atomic orbital basis:

$$n_i = \langle\phi_A|\mathbf{D}|\phi_A\rangle \qquad (2)$$

Ruedenberg further defined the kinetic bond order K_{AB} between atoms A and B in terms of QUAO overlaps and kinetic energy contributions:

$$K_{AB} = \sum_i \langle\phi_A^{(i)}|\hat{T}|\phi_B^{(i)}\rangle n_i \qquad (3)$$

where $\hat{T}$ is the kinetic energy operator and the sum runs over all occupied QUAOs. This formalism allows decomposition of bonding into atomic contributions, providing quantitative insight into hybridization, bond covalency, and delocalization effects.

Figure 8: Mathematical foundation behind quasi-atomic orbital (QUAO)

$$\rho(1,2) = \sum_{Aa}\sum_{Bb} |Aa(1)\rangle p_{Aa,Bb} \langle Bb(2)|$$

$$k_{\mathrm{Aa,Bb}} = 0.1 p_{\mathrm{Aa,Bb}} \langle \mathrm{Aa}| -\frac{1}{2}\nabla^2 |\mathrm{Bb}\rangle A \neq B$$

Figure 9: Density Bond Orders and Kinetic Bond Orders from QUAO (Rudenberg et al., 2020)

Results & Discussion

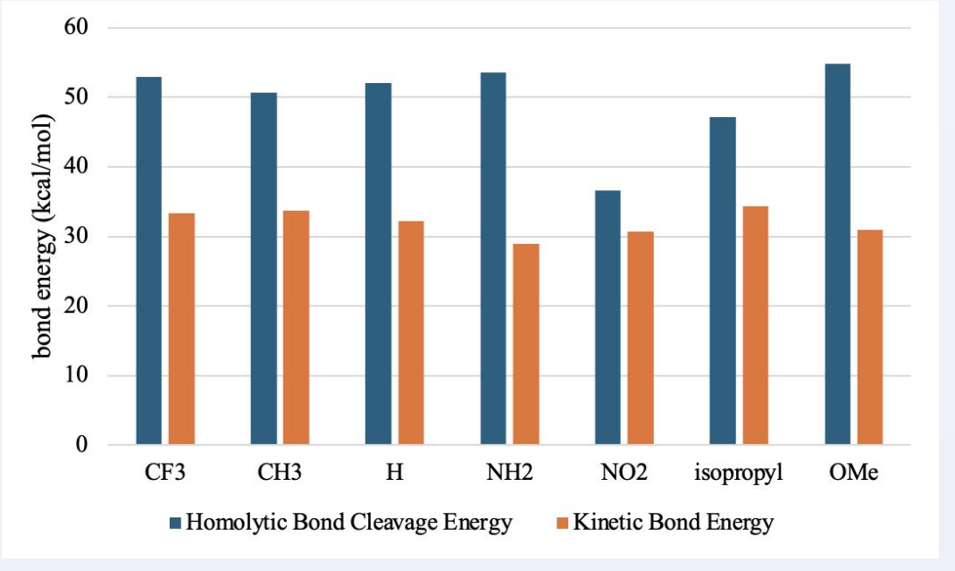

Figure 10: Homolytic bond dissociation energies of Bi-H bonds for different functional groups vs kinetic bond order (KBO)

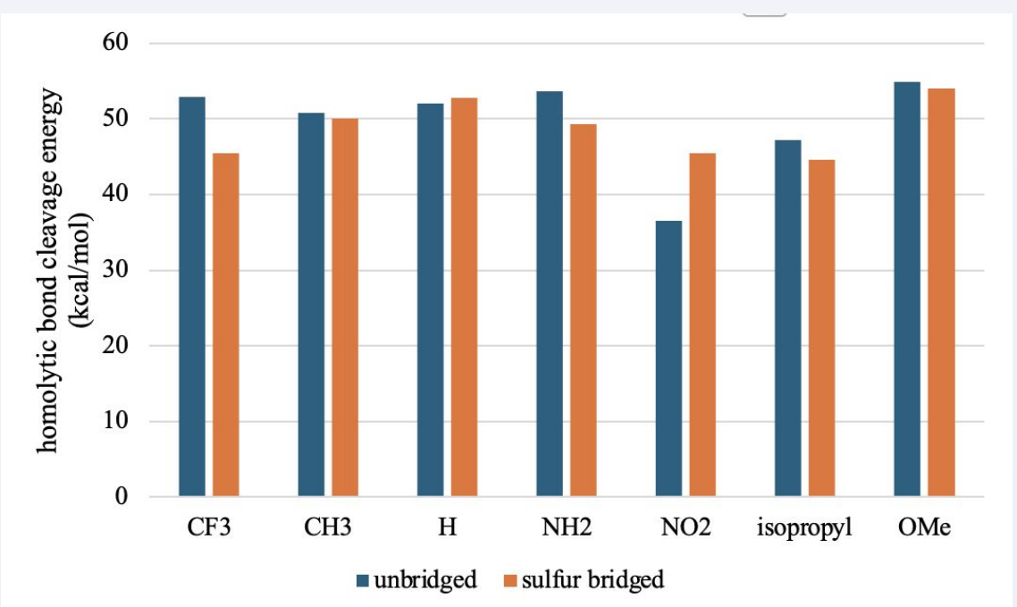

Figure 11: Difference in homolytic bond dissociation energies of Bi-H bonds between sulfur-bridged and unabridged Bi(di-aryl)SPh

Across the series of aryl substituents (CF_3 to OMe), the homolytic Bi–S bond dissociation energies (BDEs) vary substantially, spanning approximately 36–55 kcal/mol, while the corresponding kinetic bond order (KBO) values remain confined to a narrower range (~29–34). Notably, no monotonic or linear correlation is observed between KBO and homolytic BDEs.

When comparing bridged versus sulfur-bridged Bi–S bonds, distinct trends emerge. Bridged systems generally exhibit higher BDEs due to additional stabilization from the bridging framework, while sulfur-bridged bonds show more variation depending on the substituents electronic and steric effects. These differences highlight that bond strength in heavy main-group systems cannot be fully captured by either simple bond order metrics or structural classification alone.

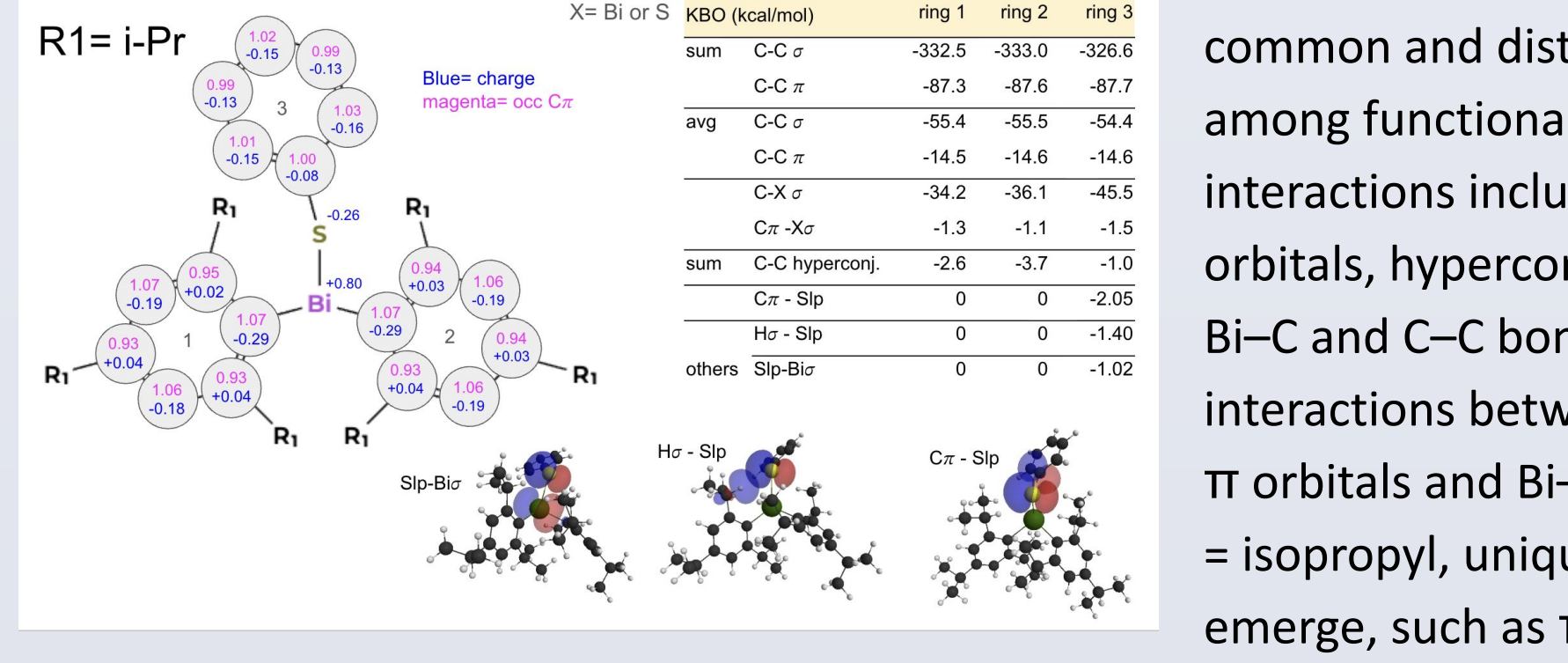

KBO (kcal/mol)		ring 1	ring 2	ring 3
sum	C-C σ	-332.5	-333.0	-326.6
	C-C π	-87.3	-87.6	-87.7
avg	C-C σ	-55.4	-55.5	-54.4
	C-C π	-14.5	-14.6	-14.6
	C-X σ	-34.2	-36.1	-45.5
	Cπ -Xσ	-1.3	-1.1	-1.5
sum	C-C hyperconj.	-2.6	-3.7	-1.0
	Cπ - Slp	0	0	-2.05
	Hσ - Slp	0	0	-1.40
others	Slp-Biσ	0	0	-1.02

Figure 12: Sample processed QUAO data of Bi(di-aryl)SPh with R_1 = isopropyl

The processed data reveals both common and distinct interactions among functional groups. Shared interactions include C–C σ and π orbitals, hyperconjugation between Bi–C and C–C bonds, and interactions between the phenyl ring π orbitals and Bi–S σ orbitals. For R1 = isopropyl, unique interactions emerge, such as π orbital–sulfur lone pair interactions, which was visualized via MacMolPlt.

KBO (kcal/mol)		ring 1	ring 2	ring 3
sum	C-C σ	-333.0	-332.9	-326.8
	C-C π	-88.3	-87.8	-87.7
avg	C-C σ	-55.5	-55.5	-54.5
	C-C π	-13.7	-13.6	-13.6
	C-X σ	-34.3	-33.0	-45.1
	Cπ -Xσ	-1.1	-1.2	-2.1
sum	C-C hyperconj.	-2.7	-2.6	-2.0
	Bi-S σ		-33.74	

CH3

KBO (kcal/mol)		ring 1	ring 2	ring 3
sum	C-C σ	-332.5	-333.0	-326.6
	C-C π	-87.3	-87.6	-87.7
avg	C-C σ	-55.4	-55.5	-54.4
	C-C π	-14.5	-14.6	-14.6
	C-X σ	-34.2	-36.1	-45.5
	Cπ -Xσ	-1.3	-1.1	-1.5
sum	C-C hyperconj.	-2.6	-3.7	-1.0
	Cπ - Slp	0	0	-2.05
	Hσ - Slp	0	0	-1.40
others	Slp-Biσ	0	0	-1.02
	Bi-Sσ		-34.33	

i-Pr

KBO (kcal/mol)		ring 1	ring 2	ring 3
sum	C-C σ	-334.1	-334.3	-326.5
	C-C π	-82.4	-83.1	-87.6
avg	C-C σ	-55.7	-55.7	-54.4
	C-C π	-13.7	-13.8	-14.6
	C-X σ	-30.7	-31.4	-44.4
	Cπ -Xσ	-1.6	-1.0	-2.4
sum	C-C hyperconj.	-2.3	-2.3	-1.0
	O-Bi		-1.27	
	Bi-Sσ		-30.94	

OCH3

Comparing the common electron-withdrawing groups (R1 = CH_3, isopropyl, and OCH_3), most interactions show no clear trend or exhibit similar values. An exception is the interaction between the π orbitals of the SPh ring and the Bi–S σ orbital, which may serve as evidence of π-backbonding.

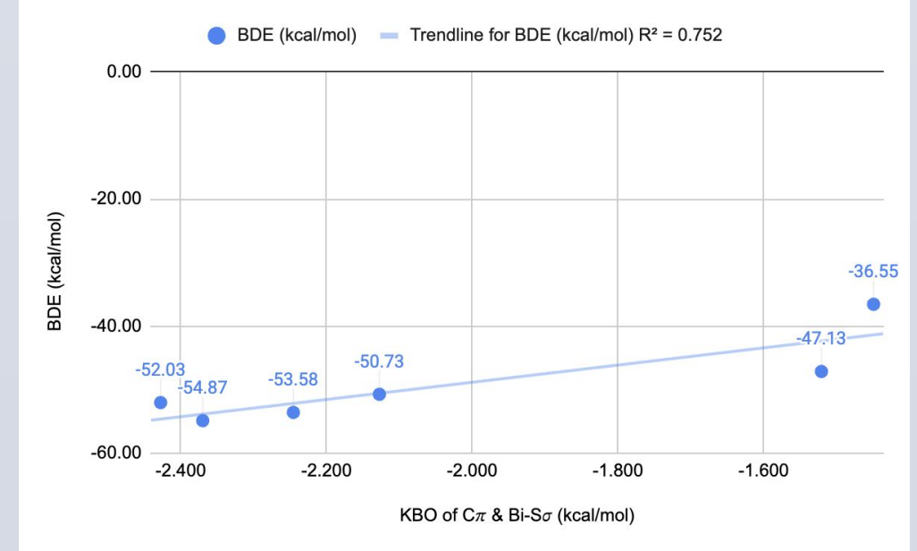

The plot of Bi–S bond dissociation energies (BDE) versus the KBO values of the π-backbonding interaction shows a clear trend: stronger σ–π interactions correspond to a stronger Bi–S bond. This relationship is further clarified by the specific QUAO data.

X=	Bond Order	KBO (kcal/mol)	BDE (kcal/mol)	I (QUAO #1 index)	OCC #1	QUAO #1	Orbital I	J (QUAO #2 index)	OCC #2	QUAO #2	Orbital J	Total OCC
isopropyl	0.875125	-34.36138828	-47.13	87	1.399882	S2(BI1)	σ	84	0.621419	BI1(S2)	σ	2.021301
CH3	0.892159	-33.73830311	-50.73	75	1.359988	S2(BI1)	σ	72	0.645386	BI1(S2)	σ	2.005374
NH2	0.855596	-28.88364055	-53.58	75	1.414825	S2(BI1)	σ	72	0.597505	BI1(S2)	σ	2.01233
OCH3	0.878349	-30.97085024	-54.87	81	1.37964	S2(BI1)	σ	78	0.631414	BI1(S2)	σ	2.011054
NO2	0.875195	-30.64423301	-36.55	87	1.376759	S2(BI1)	σ	82	0.65526	BI1(S2)	σ	2.032019
H	0.896268	-32.17430909	-52.03	69	1.344943	S2(BI1)	σ	66	0.665835	BI1(S2)	σ	2.010778

The bond order of these interactions increases alongside the KBO, clearly indicating that π-backbonding strengthens and contributes to the stabilization of the Bi–S bond. Furthermore, occupation analysis shows that the Bi–S bond holds more electron density than the π orbital, consistent with electron donation from the π system to the Bi–S bond.

In other words, the strengthening of π-backbonding from the SPh ring appears to be significant. However, since the SPh ring lacks obvious functional groups, this trend likely arises from geometric and steric effects rather than purely electronic factors. To identify the specific geometric constraints influencing BDE variation, complex structural analyses, such as heat maps, could be beneficial. Additionally, QUAO analysis of geometrically constrained structures—such as bridged systems or rings with substituents only at the para position—can help isolate and evaluate the electronic effects of those substituents.

RESEARCH POSTER PRESENTATION DESIGN © 2015
www.PosterPresentations.com